XXI IMEKO World Congress "Measurement in Research and Industry"
August 30 – September 4, 2015, Prague, Czech Republic

ELASTICITY OF MASS ARTIFACTS IN SINUSOIDAL FORCE CALIBRATION

John C. Bankert [1] *and Ako Chijioke* [2]

[1]University of Maryland, College Park, MD 20742, USA.
[2]National Institute of Standards and Technology, Gaithersburg, MD 20899, USA.
ako.chijioke@nist.gov

Abstract – Dynamic calibration of force transducers using sinusoidal acceleration of load mass objects requires the accurate determination of the displacement field in such objects, in order to relate accelerations measured at one or a few locations on the object to its body-averaged acceleration. We present the results of finite element calculations of such displacement fields, and show that there are significant differences from the results of first-order approximations at calibration frequencies above ≈ 1 kHz for typical load mass objects.

Keywords: dynamic force, force calibration, sinusoidal force, harmonic force, elastic waves.

1. INTRODUCTION

The analysis of multi-dimensional elastic wave propagation in cylinders has been undertaken since the end of the nineteenth century [1, 2] but exact analytical solutions can be obtained only for a few cases, with most cases requiring numerical modeling for accurate solutions. A problem requiring the accurate determination of displacement fields in harmonically-driven elastic cylinders is the case of sinusoidal force calibration using accelerated masses. In this technique, illustrated in Fig. 1, a body of known mass is affixed to a force transducer to be calibrated, and the two objects are accelerated together sinusoidally. The acceleration is measured, and the product of this acceleration with the known mass gives the force being applied to the transducer. Cylinders are the most-commonly used load mass shapes, and the acceleration is often measured at a single point on the free end of the load mass, such as by a laser vibrometer. The problem is to solve the elastic wave equation in a driven, finite, cylinder, with the harmonic drive applied to one end and all other surfaces free, determining the acceleration at a point on the free end. The ratio of this to the body-averaged acceleration gives a frequency-dependent correction factor to the single- point acceleration measurement. We describe here the solution of this problem for general cylinders by finite-element analysis, comparing the result to a one-dimensional analytical calculation, for drive frequencies up to 5 kHz. We also present more-accurate simulations for two specific mass objects. Kumme [3,4] has previously used finite-element modelling to determine the correction factor for steel load

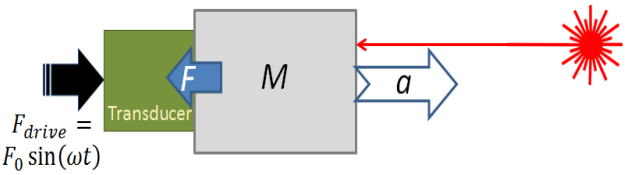

Fig. 1. Schematic of sinusoidal force calibration based on an accelerated mass. A sinusoidal drive is applied to a transducer-mass assembly, and the acceleration of the load mass object is measured, e.g. using a laser vibrometer. The force applied to the transducer is determined as the product of the object mass and its measured acceleration.

mass cylinders up to 1 kHz, and compared this to the one-dimensional analytical solution.

2. APPROXIMATE ANALYTICAL SOLUTION

A long cylinder may be approximated by a one-dimensional rod, and thereby the problem may be modeled as such a rod with one end driven and the other end free. For a rod of length L, density ρ and Young's modulus E, the equation of motion is

$$\frac{\partial^2 u(z,t)}{\partial t^2} = \frac{E}{\rho}\frac{\partial^2 u(z,t)}{\partial z^2}\,, \tag{1}$$

with boundary conditions

$$u(0,t) = A\,\cos(\omega t)\,, \tag{2}$$

$$\frac{\partial u}{\partial z}(L,t) = 0\,, \tag{3}$$

where A is the displacement amplitude of the driven end. The solution to this model is

$$u(z,t) = A\left[\cos\left(\frac{\omega z}{c_l}\right) + \tan\left(\frac{\omega L}{c_l}\right)\sin\left(\frac{\omega z}{c_l}\right)\right]\cos(\omega t)\,, \tag{4}$$

where c_l is the longitudinal wave speed $\sqrt{E/\rho}$. This yields an acceleration amplitude correction factor of

$$K_{1D} = \frac{\left[\left(\frac{1}{L}\right)\int_0^L \ddot{u}(z)dz\right]}{\ddot{u}(L)} = \left[\frac{\sin(\omega L/c_l)}{\omega L/c_l}\right]. \tag{5}$$

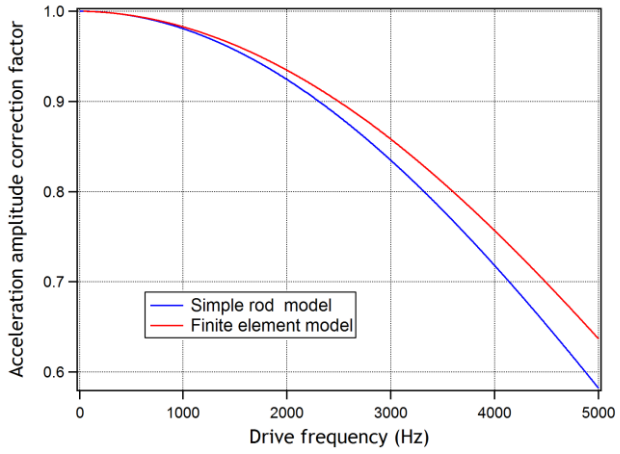

Fig. 2. Comparison of the acceleration amplitude correction factor determined from a one-dimensional model to the correction factor determined from a two-dimensional finite-element model. Results are plotted for a cylinder of mass 5 kg, length 5 × diameter, Young's modulus 200 GPa, Poisson's ratio 0.3, and density 8000 kg/m^3.

This is plotted in Fig. 2 for a 5 kg stainless-steel (E = 200 GPa, υ = 0.3, ρ = 8000 kg/m^3) cylinder of length 10 × its radius. This one-dimensional result will become increasingly inaccurate as the aspect ratio of the cylinder is reduced.

3. FINITE-ELEMENT SOLUTION

The three-dimensional elastic wave equation in an isotropic, uniform-density (and time-invariant-density) material is [5]

$$\rho\ddot{\mathbf{u}} = \mu\nabla^2\mathbf{u} + (\lambda+\mu)\nabla(\nabla\cdot\mathbf{u}), \tag{6}$$

where $\mathbf{u}$ is the displacement of a material point from its initial position, and λ and μ are the Lamé elastic constants of the material. The problem is reduced to two dimensions by assuming axisymmetry. This problem was solved by the finite-element method for the case of a cylinder harmonically driven at one end, using the *COMSOL* [6, 7] software package.

3.1 Simulation model

A cylinder of radius R and height h with uniform, isotropic material properties E, υ, ρ is driven by an axial sinusoidal force $F_0 \sin(2\pi f\, t)$ applied uniformly over a disc of radius r_a on one end. The resultant axial acceleration is measured at radial position P on the opposite end of the cylinder. The nine independent variables (R, h, E, υ, ρ, r_a, P, f, F_0) in the problem are reduced to eight by the assumption of linearity, which removes the applied force magnitude as a relevant variable. The dependence on r_a and P is found to be close to quadratic, so solutions are found for two limiting cases of each (r_a = $R/10$, R; P = 0, R), with solutions at intermediate values found by interpolation. Dimensional analysis is applied to reduce the remaining six variables to 3:

$$\pi_1 \equiv \frac{h}{2R}; (Aspect\ ratio) \tag{7}$$

$$\pi_2 \equiv \nu; (Poisson's\ ratio) \tag{8}$$

$$\pi_3 \equiv \left(\frac{h\,f}{\sqrt{K/\rho}}\right)^2 \tag{9}$$

where K is the bulk modulus, $K = E/3(1-2\upsilon)$.

Triangular elements were used for meshing and a mesh-convergence test was performed. The mesh density used in the simulations used gave correction factors within 5 × 10^{-7} of the correction factor calculated with more than 3 × the number of mesh degrees of freedom, for frequencies below 5 kHz, and within 2 × 10^{-5} for frequencies below 10 kHz. Simulations were performed for sweeps of π_1 from 1.1 to 10 in 28 steps, π_2 from -0.9 to 0.45 in 16 steps, and π_3 from the value corresponding to 25 Hz to that corresponding to 2.5 × f_0 in ≈ 300 steps, where f_0 is the first longitudinal resonance frequency of the cylinder.

3.2 Results

The correction factor is the body-averaged acceleration for the simulated applied force and cylinder mass, divided by the acceleration at the measurement point. An example is shown in Fig. 1, and is seen to differ significantly from the one-dimensional model at high frequencies (f > 1 kHz, for this aspect ratio and mass). For the plotted case, the difference is about 1 % at 2 kHz and about 5 % at 5 kHz. A database of correction factors over the range of simulated parameters (π_1, π_2, π_3, r_a, P) has been assembled, allowing interpolation to find the correction factor for a given calibration mass. The sensitivity of the correction factor to variations in the parameter values was also determined at each point, allowing uncertainty in the input parameter values to be translated into an uncertainty in the correction factor.

3.3 Uncertainty of correction factor

If the uncertainty in the input parameter values is sufficiently low, the uncertainty in the correction factor will be primarily due to un-modeled aspects (for example the exact boundary condition of the sinusoidal drive and neglected geometrical details of the mass objects) and to interpolation in the generated database of correction factors. Interpolation between simulated (r_a, P) points introduces an uncertainty (k = 2) of up to 9.6 %, predominantly (9 %) due to the driving area (r_a) interpolation. (This uncertainty does not apply to the plot shown in Fig. 2, which is for uniform drive over the whole cylinder end surface, one of the simulated data points.) Note that these uncertainty values are the uncertainty in the difference of the correction factor from 1.

4. CORRECTION FACTOR FOR SPECIFIC MASS OBJECTS

4.1 Geometry and boundary conditions

Higher-accuracy correction factors were determined for two specific load mass objects used in the sinusoidal force calibration system at NIST. These objects are shown in Fig.

Fig. 3. Specific load mass objects for which elastic properties were measured and more-detailed simulations carried out. The object on the left has a mass of approximately 1 kg, a diameter of ≈ 0.06 m, and a height of ≈ 0.045 m. The object on the right has a mass of approximately 10 kg, a diameter of ≈ 0.12 m, a height of ≈ 0.13 m and an internal cavity of depth ≈ 0.06 m. In addition to the holes shown, each mass had a threaded hole in its base of diameter 6.4 mm and depth ≈ 20 mm.

3 and had masses of 0.99837 kg and 9.99709 kg respectively, with a relative uncertainty ($k = 2$) of 6×10^{-5}. The 10 kg object has a central cylindrical cavity extending the upper half of its height, and both cylinders have small screw holes and chamfers. Three-dimensional finite-element models of these masses were constructed for determination of the acceleration correction factor.

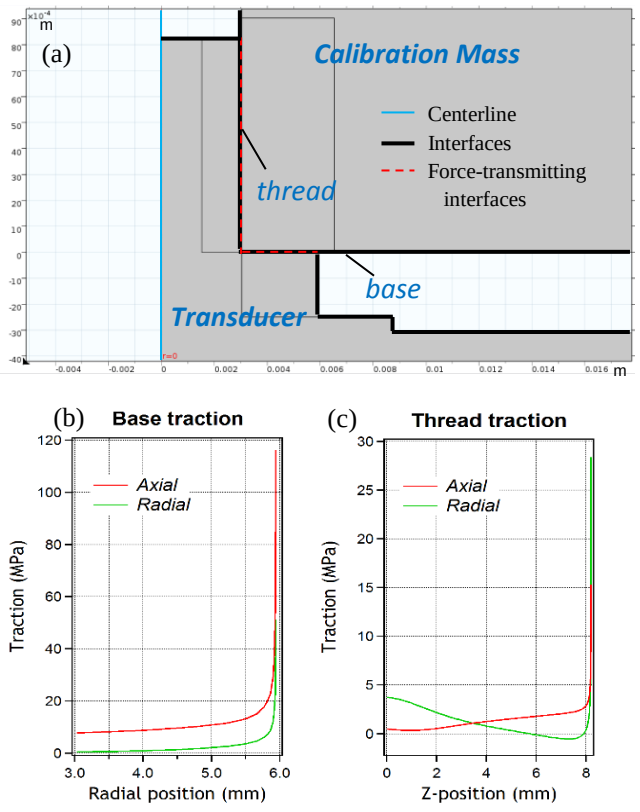

Fig. 4. Distribution of applied force on of 1 kg calibration mass. (a) Detail of mass-transducer interface. (b) Force distribution on base surface. (c) Force distribution along mounting hole thread. Note the different vertical scales.

The boundary condition at the driven end was modeled in much greater detail for these objects. The driving force is not simply applied to the base surface of each object, but partly to the threads of the mounting screw hole and partly to the base surface. The loading stress distribution is determined by constructing a two-dimensional finite-element model of the load object and a coupled force transducer as a single object, running the simulation with an external force applied to the base of the transducer, and probing the stress distribution along the spatial path corresponding to the mass object base surface and mounting hole threads. The determined stress distribution profiles are shown in Fig. 4 for the 1 kg object. We observe that the force is applied predominantly to the base of the calibration mass and is peaked at the edge of the contact area between the calibration mass and the transducer. The determined stress distribution has some dependence on the modeled transducer structure, and thus the results in this section apply to the particular transducer modeled.

4.2 Elastic moduli determination

Accurate values for the elastic properties of load masses are needed in order for accurate values of the correction factor to be determined. The elastic moduli of as-manufactured steel alloys cannot be assumed to match tabulated reference data to better than ≈ 10 %. To improve upon this, we determined the elastic constants of the two load mass objects from measurements of vibrational mode frequencies [8, 9].

The 1 kg mass was suspended by a thin wire attached to the top center hole with a nylon screw to obtain free-free boundary conditions on the mass. A small accelerometer (mass = 2.3 g) was mounted on a screw hole near the outer edge of the mass such that the accelerometer and the mass vertical axis were parallel. The load mass was struck transversely with a small ball-hammer and the accelerometer output recorded for 1 second. One hundred such impacts were recorded, and exported for analysis. These were Fourier-transformed and the 100 amplitude spectra averaged. Peak fitting using the *IGOR Pro* [7, 10] software package was used to determine the location of the observed peaks. The obtained spectrum is shown in Fig. 5.

The 10 kg load mass was supported on a rubber o-ring for the test. A small accelerometer (mass = 5.8 g) was mounted on the 10 kg mass by a screw hole. The load mass was struck transversely on its side using a small ball-hammer, and vertically on the bottom surface of the central cavity in it using a half-inch-diameter steel rod. A total of 512 impacts of each type were recorded for 0.6125 s each, and processed using the same procedure as for the 1 kg mass.

The thus-obtained spectra were compared to simulated spectra. Details of the cylinders including screw holes and chamfers were modeled, as well as the mounted accelerometers. These simulations were performed in three dimensions in order to accurately accommodate the geometry of the object, the rotational symmetry being broken by the screw holes and the accelerometers. Newton's method was used to iteratively align the simulated resonant

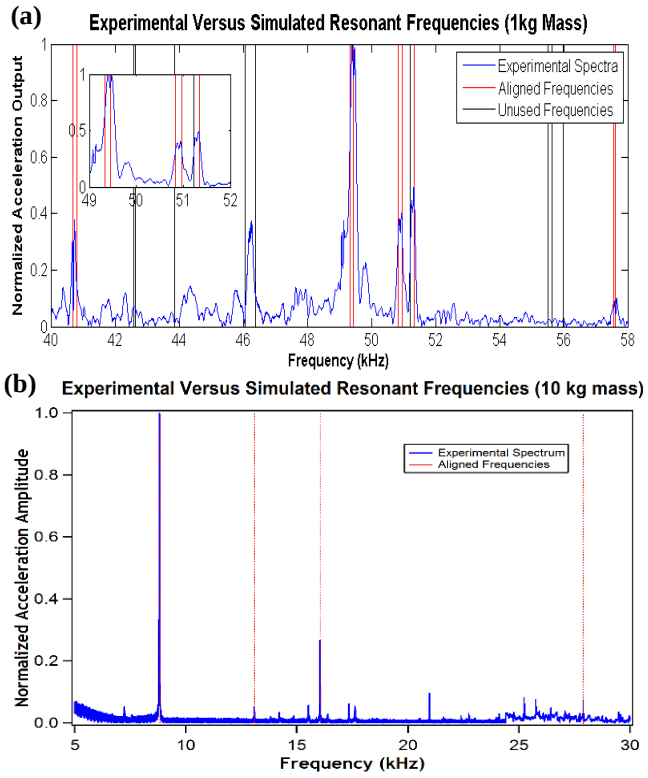

Fig 5. Measured vibration spectrum and simulated mode frequencies of specific mass objects.

frequencies with experimentally determined resonant frequencies using the cost function

$$R = \sum_j \left[\frac{1}{u_j\, \omega_j} \left(\delta\omega_j - \left(\frac{\partial \omega_j}{\partial E}\, \delta E + \frac{\partial \omega_j}{\partial \upsilon}\, \delta\upsilon \right) \right) \right]^2, \qquad (10)$$

where ω_j are the experimentally measured resonance frequencies, $\delta\omega_j$ are the differences between the experimental resonance frequencies and the corresponding simulated resonance frequencies and u_{j1} is a weighting factor corresponding to the uncertainty $\Delta\omega_j$ of the mode frequency ω_j:

$$u_{j1} = \frac{\Delta\omega_j/\omega_j}{\sqrt{(1/n)\sum_{k=1}^{n}(\Delta\omega_k/\omega_k)}}. \qquad (11)$$

Uncertainties due to the experimental resonant frequency measurement, finite simulation convergence and object dimensional measurements, contribute to u_{j1}, and these uncertainties are described in the next section. Starting from initial guesses (E = 180 GPa, υ = 0.35) for the elastic moduli, simulated values of the resonant frequencies were determined, and thereby the differences $\delta\omega_j$. $\left(\frac{\partial\omega_j}{\partial E}, \frac{\partial\omega_j}{\partial\upsilon}\right)$ were computed by slightly varying (2 % difference) each modulus in turn and observing the shifts in the simulated resonance frequencies[1]. The two equations $\partial R/\partial\delta E = 0$, $\partial R/\partial\delta\upsilon = 0$ were next solved to determine (δE, $\delta\upsilon$), which were added to the starting moduli values. The process was repeated until the indicated relative change in each modulus was less than 1×10^{-5}.

This process is somewhat computationally intensive, and many iterations of the process were required to obtain a converged solution. Including the soft o-ring in the simulation for the 10-kg object yielded numerous modes of the o-ring, making it difficult to find the mass eigenfrequencies among them. In the final simulations, the o-ring was not included, but a correction to the resonant peak frequencies was introduced to account for its effect. This correction factor was determined by running the simulation once with the o-ring and once without the o-ring, for a fixed pair of values for E and υ. The difference of this corrective multiplier from 1 ranged from 1.3×10^{-5} to 9.9×10^{-5} for the resonance peaks used.

For the 1 kg object, nine simulated modes were found to line up with the experimental data, as shown in Fig. 5. These included four pairs of transverse modes and one single transverse mode (determined by looking at the simulated mode deformation pattern). For the 10 kg object, comparing simulation to experimental data yielded five peaks with good correlation. One of these four peaks was the first longitudinal mode, while the remainder were transverse modes. The corresponding elastic moduli were determined as (E = 198.5 ± 0.36 GPa, υ = 0.275 ± 0.0033) for the 1 kg object and (E = 197.9 ± 1.63 GPa, υ = 0.290 ± 0.037) for the 10 kg object. The quoted uncertainties are k = 2 expanded uncertainties, determined as discussed next.

4.3 Uncertainty of measured elastic properties

The relative uncertainty for each elastic modulus was determined by a weighted sum of the contributions from all used resonant frequencies,

$$\frac{\Delta\eta}{\eta} = \sqrt{\frac{\sum_{j=1}^{n}\left[\frac{1}{u_{j2}}\left(\frac{\partial\eta}{\partial\omega_j}\Big/\frac{\eta}{\omega_j}\right)\frac{\Delta\omega_j}{\omega_j}\right]^2}{n-2}}, \qquad (12)$$

where η is the elastic modulus (E or υ), n is the number of vibrational modes used, ω_j are the mode frequencies, $\Delta\omega_j$ are the uncertainties assigned to each mode frequency, and the 2 in the denominator is because two elastic constants are determined by the optimization. The quantity u_{j2} is similar to u_{j1}, but includes an additional uncertainty contribution to the mode frequency due to residual mismatch between the experimental and simulated frequencies, discussed further below.

There are four contributions to the $\Delta\omega_j$, namely: experimental uncertainty – uncertainty in the measured vibrational mode frequencies; simulation uncertainty – numerical uncertainty in the calculated mode frequencies; dimensional uncertainty – uncertainty in the calculated mode frequencies due to uncertainty in the measured object dimensions and mass; and residual uncertainty – an additional uncertainty added to account for residual mismatch between measured and simulated resonant frequencies. These contributions and the resulting mode frequency uncertainties are shown in Table 1. The experimental uncertainty $\Delta\omega_{j,exp}$ is determined as the

[1] For Young's modulus E, if the simulated structure is made of a single material then the resonant frequencies are proportional to $E^{1/2}$, and $\partial\omega_j/\partial E = \omega_j/2E$ exactly. However we do not use this as the accelerometers in the simulation are not made of the same material as the calibration masses.

Table 1. Resonant mode frequencies used in the elastic property determination, and uncertainties in these frequencies.

ω_j [Hz]	$\Delta\omega_{j,exp}/\omega_j$	$\Delta\omega_{j,sim}/\omega_j$	$\Delta\omega_{j,dim}/\omega_j$	$\Delta\omega_{j,res}/\omega_j$	$\Delta\omega_j/\omega_j$
1 kg mass resonances:					
40665	2.9E-5	2.0E-5	1.2E-4	7.3E-4	7.4E-4
40751	2.9E-5	1.9E-5	1.2E-4	1.2E-3	1.2E-3
49381	3.0E-5	3.8E-5	1.3E-4	9.2E-4	9.3E-4
49492	2.9E-5	3.8E-5	1.3E-4	9.4E-4	9.5E-4
50852	1.1E-4	4.2E-5	1.4E-4	2.6E-4	3.2E-4
50941	7.7E-5	2.6E-5	1.4E-4	5.9E-4	6.1E-4
51325	4.2E-5	5.1E-5	1.1E-4	3.6E-4	3.8E-4
57575	2.6E-5	7.4E-5	1.2E-4	5.3E-5	1.5E-4
57656	1.9E-5	6.8E-5	1.2E-4	7.0E-4	7.1E-4
10 kg mass resonances:					
8798.2	3.0E-5	3.2E-4	1.1E-4	3.7E-4	5.0E-4
8813.0	1.7E-5	3.0E-4	1.1E-4	3.4E-3	3.4E-3
13085	4.8E-5	1.0E-3	6.7E-5	6.1E-4	1.2E-3
16046	1.1E-5	2.2E-5	6.2E-5	6.4E-4	6.4E-4
27897	1.7E-5	3.5E-5	6.0E-5	2.1E-4	2.2E-4

standard deviation of the fitted peak center. The simulation uncertainty $\Delta\omega_{j,sim}$ is determined as the difference between the simulated frequencies at the used mesh density and at a mesh density with a factor of 2 fewer degrees of freedom[2]. This difference is larger than the difference between the simulated frequencies with the used mesh density and with a mesh density with a factor of 2 increase in the number of degrees of freedom. The dimensional uncertainty $\Delta\omega_{j,dim}$ is determined as

$$\frac{\Delta\omega_{j,dim}}{\omega_j} = \sqrt{\sum_{i=1}^{n_d}\left[\left(\frac{d_i}{\omega_j}\frac{\partial\omega_j}{\partial d_i}\right)\frac{\Delta d_i}{d_i}\right]^2}, \qquad (13)$$

where d_i is the i^{th} dimension, Δd_i is the uncertainty of the dimensional measurements, and n_d is the number of dimensions. The final component $\Delta\omega_{j,res}$ is equal to the residual mismatch between the simulated peak frequency and experimental peak frequency after the iterative optimization. For most of the resonant frequencies this residual difference is the largest component of the uncertainty. This residual difference may result from unmodeled phenomena.

4.4 Correction factor results

Results for the simulated correction factors for these two mass objects are shown in Fig. 6 up to 5 kHz. For the 1 kg mass, the correction factor for measurements at the center of the top surface is ≈ 1.2 % at 5 kHz. For the 10 kg mass, the correction factor for measurements at the inner diameter edge is ≈ 16 % at 5 kHz. The $k = 2$ relative uncertainty of the difference of the correction factor from 1 is 0.007 for the 1 kg mass and 0.016 for the 10 kg mass. These uncertainties are determined by considering the uncertainty in the mass

[2] The exception to this is the 13085 Hz mode of the 10 kg mass, for which two nearly-degenerate modes were found in the simulation. There was no means to select one of the two as the correct one, and therefore the uncertainty in the peak frequency is taken as half the frequency difference between the two modes.

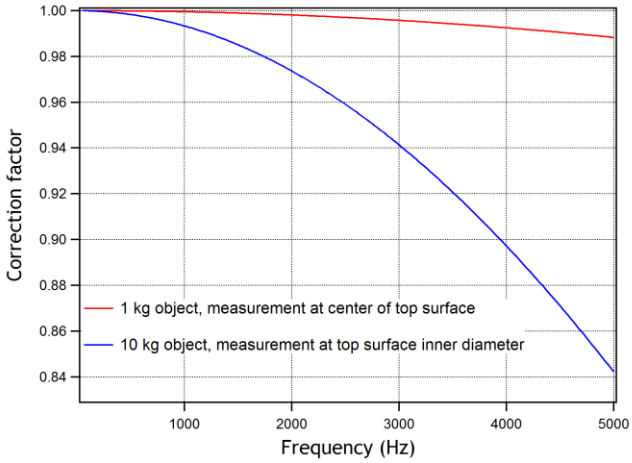

Fig. 6. Calculated correction factors from detailed simulations of specific 1 kg and 10 kg mass objects.

object parameters (dimensions, mass and elastic properties) and the sensitivities of the calculated correction factors to these input parameters. The uncertainty in the elastic properties (especially υ) is the dominant contribution.

5. CONCLUDING REMARKS

We have observed that sinusoidal force calibration based on the acceleration of kilogram-range load mass objects in the kilohertz frequency range requires multidimensional solutions of the elastic wave equation for accurate determination of the acceleration distribution. Acceleration amplitude correction factors for generalized cylinders with aspect ratios ranging from 1.1 to 10 were calculated by two-dimensional finite-element modelling. More-detailed simulations to determine more-accurate correction factors were performed for the two objects shown in Fig. 3, which included geometrical details such as chamfers and axial holes, and detailed modelling of the distribution of the applied force on the bottom surface and mounting thread.

The remaining uncertainty in the correction factor in these detailed simulations is set by uncertainty in the input parameters, predominantly uncertainty in the elastic moduli, and is in the range of 1 % of the difference of the correction factor from 1 (thus at most a few parts in 1000 of the measured calibration mass acceleration for the frequency range up to 5 kHz). This uncertainty can be reduced by more accurate determination of the input parameters, but will ultimately be limited by modelling approximations. In the present case such approximations included neglecting damping, the assumptions of linear elasticity and material isotropy, and modelling the undriven surfaces as free (i.e. neglecting air drag).

ACKNOWLEDGMENTS

We gratefully acknowledge the advice of R. Ricker of NIST on measurements of elastic constants. We thank R. Kumme of Physikalisch-Technische Bundesanstalt, Germany, for providing us with copies of his related publications.

Official contribution of the National Institute of Standards and Technology; not subject to copyright in the United States.

REFERENCES

[1] L. Pochhammer, "On the propagation velocities of small oscillations in an unlimited isotropic circular cylinder" ("Ueber die Fortpflanzungsge-schwindigkeiten kleiner Schwingungen in einem unbegrenzten isotropen Kreiscylinder"), *Journal für die reine und angewandte Mathematik*, vol 81, pp. 324-336, 1876.

[2] C. Chree, "The equations of an isotropic elastic solid in polar and cylindrical coordinates, their solutions and applications," *Trans. Camb. Phil. Soc. Math. Phys. Sci.*, vol 14, p. 250, 1889.

[3] R. Kumme, "The determination of the effective dynamic force for the calibration of force transducers, with due regard to the distribution of mass and acceleration," *IMEKO 15th International TC3 Conference*, pp. 129-138, Madrid, Spain, 1996.

[4] R. Kumme, *Investigation of a primary method for a dynamic calibration of force measuring instruments: a contribution to reduce the measuring uncertainty* (*Untersuchungen eines direkten Verfahrens zur dynamischen Kalibrierung von Kraftmeßgeräten – ein Beitrag zur Verringerung der Meßunsicherheit*), Doctoral Thesis TU Braunschweig, PTB-Bericht MA-48, 1996.

[5] L. D. Landau and E. M. Lifshitz, *Theory of Elasticity*, Pergamon Press, 1970.

[6] COMSOL Multiphysics, COMSOL Ab., Stockholm, Sweden. Version 4.3 used.

[7] Certain commercial equipment, instruments, or materials are identified in this article in order to describe the experimental procedure adequately. Such identification is not intended to imply recommendation or endorsement by the National Institute of Standards and Technology, nor is it intended to imply that the materials or equipment identified are necessarily the best available for the purpose.

[8] ASTM standard E 1876-00: *Standard Test Method for Dynamic Young's Modulus, Shear Modulus, and Poisson's Ration by Impulse Excitation of Vibration*, ASTM, West Conshohocken, PA 19428, USA, 2001.

[9] J. Han, A. Bertram, J. Olschewski, W. Hermann and H. G. Sockel, "Identification of elastic constants of alloys with sheet and fibre textures based on resonance measurements and finite element analysis," *Materials Science and Engineering*, vol A191, pp. 105-111, 1995.

[10] IGOR Pro, WaveMetrics Inc., Lake Oswego, Oregon, USA. Version 6.30 used.